

Optical properties of Ge and Si nanocrystallites from *ab initio* calculations.

II. Hydrogenated nanocrystallites

H.-Ch. Weissker, J. Furthmüller, and F. Bechstedt

Institut für Festkörperteorie und Theoretische Optik, Friedrich-Schiller-Universität, 07743 Jena, Germany

(Received 31 July 2001; revised manuscript received 7 December 2001; published 11 April 2002)

We present parameter-free calculations of the frequency-dependent dielectric function in order to understand the optical properties of Ge and Si nanoparticles. The calculations are based upon the independent-particle approximation and a pseudopotential-plane-wave method. The nanoparticles are described by clusters of up to 363 atoms. Their surfaces are passivated by hydrogen atoms. We study the size dependence of the resulting optical spectra and, especially, of the oscillator strengths of transitions near the absorption edge. In the framework of an effective-medium theory the change of the optical properties due to embedding in other environments is discussed in the light of recent measurements, e.g., of Ge nanocrystals in a sapphire matrix.

DOI: 10.1103/PhysRevB.65.155328

PACS number(s): 78.66.Db, 73.22.-f, 73.21.-b

I. INTRODUCTION

The study of germanium and silicon quantum dots or nanocrystals is a very active field of research due to the interesting fundamental physical properties and the promising applications in advanced electronic and optoelectronic devices. The optical properties have been studied intensively for frequencies near the fundamental energy gap in these nanostructures, in particular, with respect to photoluminescence (PL).¹⁻⁴ There is considerable experimental and theoretical evidence for quantum-confinement effects on PL from quantum-confined excitons.⁵ The theoretical activities were, therefore, focused on the accurate prediction of the optical energy gap for a given nanoparticle size.

The majority of the existing theoretical calculations on Si nanocrystals are of a semiempirical nature.⁶⁻⁸ They are based on the knowledge of the electronic structure of bulk silicon. However, the transferability of bulk electronic interaction parameters to a nanocrystalline environment has to be questioned.⁹ This holds for both the tight-binding approximation and the empirical-pseudopotential approach. By now, calculations have also been performed using an *ab initio* technique based on the density-functional theory (DFT) and the local-density approximation¹⁰ (LDA) or using time-dependent LDA.¹¹ Many-body effects like self-energy corrections and excitonic effects have also been taken into account.^{12,13} However, there is still a controversy about the correct treatment of the many-body effects in the calculation of the electron-hole pair excitation energies.¹⁴⁻¹⁶

Calculations of optical absorption spectra including many-body effects are rather rare and restricted to Si clusters with a maximum number of 14 Si atoms.¹⁷ Semiempirical tight-binding approaches^{18,19} allow the treatment of larger clusters. The maximum number of Si atoms handled in an empirical pseudopotential approach was much higher.^{20,21} Using *ab initio* pseudopotentials and a minimum sp^3 basis for the expansion of the wave functions, Noguez and Ulloa²² calculated absorption spectra for Si clusters of up to 70 atoms. On the other hand, optical characterizations have been done by reflectance and absorption spectroscopy in a wide frequency range of oxidized Si nanocrystallites²³ and Ge

nanocrystals of varying sizes embedded in an insulating sapphire matrix.²⁴⁻²⁶ The observed influence of the quantum size effects on the observed higher optical transitions E_1 and E_2 (Ref. 27) has recently been confirmed for E_1 by resonant Raman-scattering experiments.²⁸

The Ge and Si nanocrystallites are usually embedded in amorphous SiO_2 or Al_2O_3 matrices, or they are oxidized.^{1-5,23-26,28} One can assume that the surface dangling bonds of the nanocrystallites are saturated. In this paper, therefore, we study the frequency-dependent dielectric function of spherical Ge and Si nanocrystals passivated by hydrogen atoms. This passivation is assumed to model amorphous insulating hosts with wide energy gaps and, hence, extremely large energy barriers for electrons and holes in the group-IV nanocrystallites. The more complicated situation of a crystalline environment with smaller energy barriers or even a type-II-heterostructure behavior has been studied in part I of this paper.²⁹ The theoretical methods have also been described there in detail. Here, in Sec. II, we only give a brief summary of the methods. The results are discussed in Sec. III. Conclusions are summarized in Sec. IV.

II. MODEL AND METHOD

The electronic-structure calculations are based on the DFT-LDA. The electron-ion interaction is described by non-norm-conserving pseudopotentials, and the wave functions are expanded into a plane-wave basis set. We use the VIENNA *ab initio* SIMULATION PACKAGE.³⁰ The optical functions of the nanocrystals are evaluated within the independent-particle approximation.³¹ The optical transition matrix elements are calculated using all-electron wave functions for the valence electrons. They are constructed within the projector-augmented wave method.³² Self-energy and excitonic effects are disregarded. One justification for this approach is the tight-binding result of Delerue *et al.*¹³ that self-energy effects and Coulomb attraction partially cancel each other for not too small and not too large nanocrystal radii.

Each of the Ge and Si nanocrystals is situated at the center of a supercell. The supercells form an artificial simple-cubic (sc) crystal. We consider large sc supercells with nominally 1000 atoms in the bulk limit, i.e., supercells with an

edge length of about 2.8 nm in the Ge case. They allow the treatment of nearly spherical nanocrystals with 5, 17, 41, 83, 147, 239, and 363 group-IV atoms and a corresponding number of passivating hydrogen atoms. The majority of the results is obtained using supercells with nominally 512 atoms. For the purpose of comparison we also use cells corresponding to 216-atom supercells. The atoms are assumed to be tetrahedrally coordinated with distances 2.44 Å (Ge) and 2.34 Å (Si) taken from the bulk crystals. The assumptions of tetrahedral coordination and the conservation of the bulk bond lengths are in agreement with experimental findings for group-IV clusters with diameters of 3-7.5 nm.³³ The Ge-H and Si-H bond lengths have been optimized to find the lowest total energy of the system. The effective nanocrystal diameters (without hydrogen) are 0.60 (0.57), 0.90 (0.86), 1.20 (1.15), 1.52 (1.46), 1.84 (1.77), 2.17 (2.08), and 2.50 (2.39) nm for the corresponding Ge (Si) nanocrystals. Since the resulting energy bands are practically dispersionless we perform the sum over Bloch wave vectors in the dielectric function [cf. expression (1) in part I] using one point in the irreducible part of the Brillouin zone. The Dirac δ functions in the imaginary part of the dielectric function are broadened. We apply a constant Lorentzian broadening $\gamma=0.2$ eV to the electron-hole pair energies.

III. RESULTS AND DISCUSSION

A. Quantum size effects

The absorption edge of the nanocrystallites is characterized by transitions between the highest occupied molecular orbital (HOMO) and the lowest unoccupied molecular orbital (LUMO). We have calculated the corresponding transition energy E_g using a special Δ -self-consistent field (Δ SCF) method.^{12,14} The total energies are calculated within DFT-LDA. However, instead of calculating the electron affinity and the ionization energy individually from total-energy differences,¹² we consider the total energy of an excited electron-hole pair. This is possible by requiring the occupation number of the energetically highest Kohn-Sham eigenstate (the HOMO), occupied with two electrons in the ground state of the nanocrystal, to be 1, while one electron is placed into the LUMO state. (This applies to calculations disregarding spin.) The change of the resulting total energy of the nanocrystal with an excited electron-hole pair with respect to that of the ground state gives the pair excitation energy E_g including many-body effects. The results are plotted in Fig. 1 against the radius of the nanocrystallites. Interestingly, the pair excitation energies are not much larger than the single-particle HOMO-LUMO gaps estimated by means of the Kohn-Sham eigenvalues. A similar observation has been made by Delerue *et al.*¹³ For the considered crystallite sizes, E_g varies between 5 (6) and 1 (2) eV for Ge (Si) nanocrystals. The decrease of the transition energies with the nanocrystal size is rather rapid. We observe $E_g = E_g^{bulk} + \alpha(\text{Å}/R)^l$ with $\alpha=14.7$ eV and $l=1.0$ for Ge and $\alpha = 14.8$ eV and $l=1.0$ for Si. The pair excitation energies are smaller in Ge. In the interesting size range the Si energies are larger by about 0.5 eV. This value corresponds roughly to the difference of the fundamental energy gaps in the bulk limit.

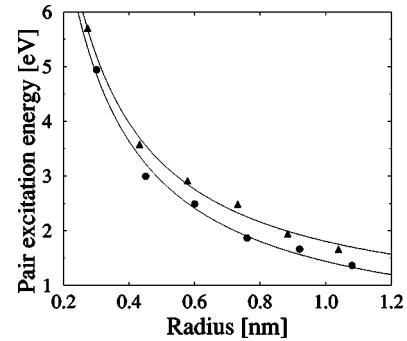


FIG. 1. Lowest electron-hole pair excitation energies of Ge (dots) and Si (triangles) nanocrystals. The solid lines are fit curves according to $E_g(R) = E_g^{bulk} + \alpha(\text{Å}/R)^l$.

In agreement with other calculations for silicon¹² we find the gap energies to vary approximately like the inverse nanocrystal radius. This is much weaker than expected from the quantum mechanics of the three-dimensional spherical potential well. The absolute values of the calculated pair excitation energies are also in rough agreement with calculated and measured excitonic energy gaps in Si dots (cf. Ref. 21). The electron-hole interaction and the reaction of the electronic system is included in our Δ SCF calculation on the DFT-LDA level of the total energy. The small underestimation of the computed values in comparison to measurements may be traced back to the similarity of the symmetry and the localization radius of the electron and hole orbitals, as discussed below. This similarity reduces the electronic relaxation of the system and, hence, tends to underestimate the gaps. Tentative calculations show that after inclusion of lattice relaxation, the HOMO state is changed and the probability distributions to find an electron or hole become different. The discrepancy between our Δ SCF values and those of Ögüt *et al.*¹² is a consequence of the inclusion of the electron-hole interaction. This attractive interaction, which takes place in the optical absorption and in luminescence experiments, lowers the pair excitation energies.^{34,35}

Figure 2 shows optical spectra of spherical nanocrystals with 5, 17, 41, 83, 147, 239, and 363 Ge or Si atoms. The absorption spectrum for the smallest Si cluster of five atoms shows the same basic features as obtained in a more sophisticated calculation.¹⁷ However, the model atomic structure used is somewhat unrealistic, and important many-body effects are not included. For that reason, we focus our attention on the larger nanocrystals, which, despite their different numbers of atoms, exhibit spectra with similar line shapes. The principal line shapes resemble those found within an empirical-pseudopotential approach for Si.²⁰

The spectra in Fig. 2, in particular, those representing the imaginary part of the dielectric function, are strongly influenced by quantum-confinement effects. The absorption threshold moves to lower energies with increasing nanocrystal size. The Kohn-Sham HOMO-LUMO gap is indicated by the arrows. Different effects of spatial quantization are observable for the main absorption structures, shoulders, or peaks for energies below 5 (6) eV (within the DFT-LDA scheme) for Ge (Si) as nanocrystal material. In the case of Ge, the shoulder at the low-energy side close to the HOMO-

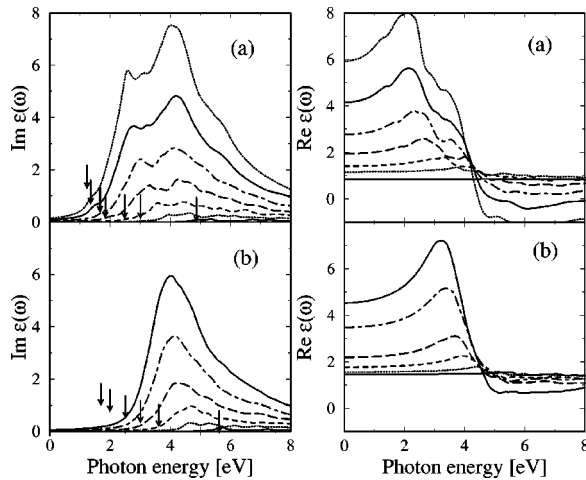


FIG. 2. Dielectric functions of Ge (a) and Si (b) nanocrystallites with a varying number N of atoms. $N=5$, solid line; $N=17$, dotted line; $N=41$, dashed line; $N=83$, long-dashed line; $N=147$, dot-dashed line; $N=239$, solid line; and $N=363$, dotted line. The vertical arrows in the absorption spectra indicate the single-particle HOMO-LUMO gaps.

LUMO gap shifts strongly towards smaller energies with increasing crystallite size. This shoulder seems to be a consequence of the strong optical transitions, which develop into the E_0 structure in the bulk limit. The first direct E_0 transition in Ge bulk crystals is energetically only slightly above the indirect energy gap.²⁷ The first peak in the 3-eV range, which also varies remarkably with the size, seems to develop into the bulk E_1 structure. Its oscillator strength is underestimated because excitonic effects are neglected in the independent-particle approach. The peak shifts from 3.6 eV (41-atom cluster) to 2.6 eV (363-atom cluster) using the DFT-LDA single-particle eigenvalues. The main peak with a maximum around 4 eV shifts much less towards smaller photon energies and develops into the E_2 structure of the bulk spectra. There is a weaker peak or shoulder at the high-energy side at about 6 eV. In the bulk case it corresponds to a structure that appears only weakly in the experimental spectra. Commonly it is related to different transitions, e.g., $\Lambda_{3v} \rightarrow \Lambda_{3c}$ and $\Delta_{5v} \rightarrow \Delta_{2'c}$.³⁶

In the Si case the confinement effects are less visible in the absorption spectra, at least within the used independent-particle approach. This can be seen from the imaginary part of the dielectric function in Fig. 2. Only one broad structure appears with a maximum between 5 and 6 eV. It exhibits a small shift of the main peak towards smaller photon energies with increasing nanocrystal size. The structure seems to develop into the bulk E_2 peak. In the case of the largest nanocrystals we considered, the almost complete absence of the E_1 structure may be related to neglecting the excitonic effects. The Coulomb effects enhance the oscillator strength of the E_1 peak but reduce the strength of the E_2 peak.³⁷ The overall line shape of the spectra in Fig. 2(b) is similar to that observed for oxidized Si nanoparticles.²³ We observe that the line shapes calculated for Si using the empirical-pseudopotential scheme²⁰ or, for Ge, using the semiempirical

tight-binding method,¹⁹ are similar. The results for fullerene-like Si nanocrystals are, however, different.²²

B. Oscillator strengths

The nanocrystal size influences not only the energetical positions of the optical transitions but also their oscillator strengths. This is clearly demonstrated in Fig. 3. It presents the optical transitions at the center of the irreducible part of the Brillouin zone. The oscillator strengths $f_{cv}^{\alpha\alpha}(\mathbf{k})$ calculated according to expression (2) of part I (Ref. 29) are plotted as vertical lines against the transition energies. The imaginary part of the corresponding normalized dielectric function is plotted to guide the eye. Figures 3(a) and 3(b) clearly show the quantum size effects on the electronic wave functions. They indicate drastic differences in the behavior of the oscillator strengths near the absorption edges. In the case of Si nanocrystals [Fig. 3(b)] with diameters above 1.5 nm a tail of weak transitions appears just above the HOMO-LUMO gap. The oscillator strengths of these transitions are much smaller than the maximum oscillator strengths of about 0.4. The occurrence of the tail can be interpreted as an indication of the development of bulk properties with increasing nanocrystal size. In bulk Si the lowest optical transitions are forbidden by the \mathbf{k} -selection rule. On the other hand, the high oscillator strengths at energies slightly above 3 eV in Si nanocrystals with 83, 147, and 239 atoms may be considered as an indication for the formation of strong direct high-energy transitions in bulk silicon.

The behavior of the oscillator strengths of transitions near the HOMO-LUMO gaps in Ge nanocrystals [Fig. 3(a)] is completely different. Very strong transitions occur close to the absorption edge, even for clusters with a diameter of about 2.2 nm. These transitions could be related to the formation of an E_0 -like absorption feature in the more extended Ge nanocrystallites. A strong near-infrared luminescence has been observed for Ge nanocrystals in a SiO_2 matrix.⁴

Since the energy region just around the HOMO-LUMO gap determines not only the absorption properties but also the luminescence properties, we study the corresponding optical transitions in detail in Fig. 4 for Ge clusters with 41, 147, and 239 atoms. Interestingly, the HOMO-LUMO transition is forbidden by symmetry. In contrast, the transition from the threefold degenerate second-highest state into the nondegenerate LUMO state possesses an extremely large oscillator strength. We observe similar results for the larger 363-atom Ge nanocrystal. The HOMO-LUMO transition remains forbidden and the transition with a slightly larger transition energy possesses a considerable strength. Interestingly, test calculations show that after atomic relaxations of the nanocrystallites the HOMO-LUMO transition becomes that with the largest oscillator strength.

The behavior of the oscillator strengths in Fig. 4 can be understood in view of the localization and the symmetry of the contributing wave functions. Strong optical transitions cannot take place between states of the same symmetry due to the usual selection rules. This can be verified by looking at the two-dimensional representations of the wave function squares in Fig. 5. It is thus not surprising to find the transi-

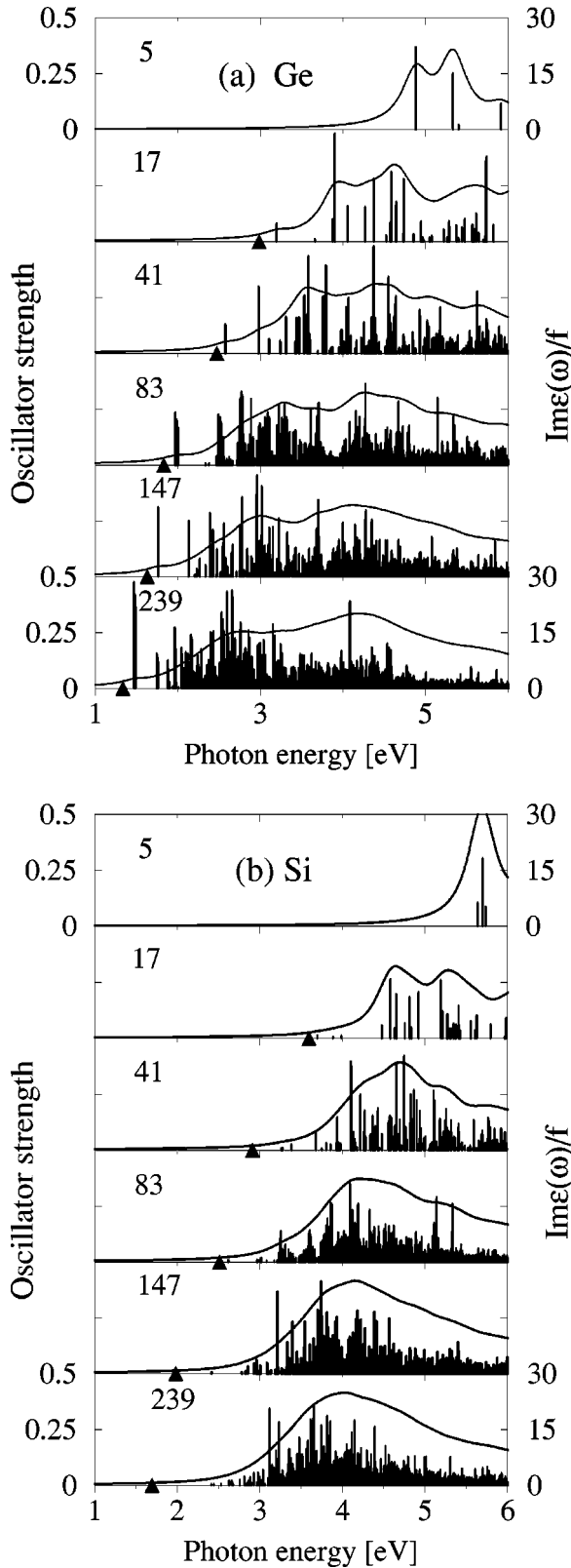


FIG. 3. Oscillator strengths of the optical transitions (vertical lines) versus the transition energies for Ge (a) and Si (b) crystallites with varying size. The normalized absorption spectrum $\text{Im}\epsilon(\omega)/f$ (solid line) is plotted to envelope the oscillator strengths. The number of atoms is indicated for each crystallite. A triangle indicates the HOMO-LUMO gap.

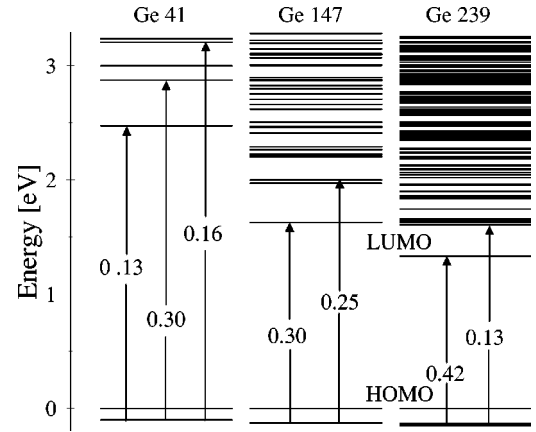


FIG. 4. Level scheme with Ge nanocrystals with 41, 147, and 239 atoms. The HOMO level defines the energy zero. The allowed optical transitions are indicated by vertical arrows. We show those with an oscillator strength larger than 0.1. The very lowest transitions have oscillator strengths, being smaller at least by two orders of magnitude. The oscillator strength of a given transition is indicated by the number at the corresponding arrow. All the shown transitions are threefold degenerate.

tion between them to be forbidden. On the other hand, the second-highest occupied state, which is also threefold degenerate, exhibits a different symmetry. Since its maximum is located at the supercell center, it exhibits transformation properties reminiscent of an s orbital, whereas the threefold degenerate HOMO state and the LUMO state have similarities with p orbitals. These symmetries may explain the selection rules discussed in Fig. 4.

C. Isolated versus embedded nanocrystals

Until now we have considered the properties of the supercell arrangement, i.e., of the composite medium of nanocrystals and vacuum. In order to extract the dielectric function $\epsilon_{nc}(\omega)$ pertaining to the nanocrystals we use the simple superposition formula

$$\epsilon(\omega) = f\epsilon_{nc}(\omega) + (1-f)\epsilon_{host}(\omega). \quad (1)$$

The quantity $\epsilon_{nc}(\omega)$ represents the optical properties of an effective bulk material which also reflects the quantum size effects characterized by a fixed nanocrystal radius R . Therefore, $\epsilon_{nc}(\omega)$ obtains its meaning only with respect to embedding in surrounding materials with possibly different filling factors but fixed nanocrystal radius. According to the independent-particle expression of the dielectric function in part I of this paper,²⁹ formula (1) should be nearly exact if the wave functions of the electrons of the nanocrystallite and the host material are strongly localized. This should be fulfilled in the case of vacuum as the host material. Indeed, expression (1) has been found to yield excellent and reproducible results. We have tested Eq. (1) by deriving $\epsilon_{nc}(\omega)$ for nanocrystals from different supercells. The corresponding dielectric functions of the composite materials have been calculated for one and the same nanocrystal but in supercells of different size. The dielectric function $\epsilon_{nc}(\omega)$ of the crystallite has been extracted using expression (1). We do not

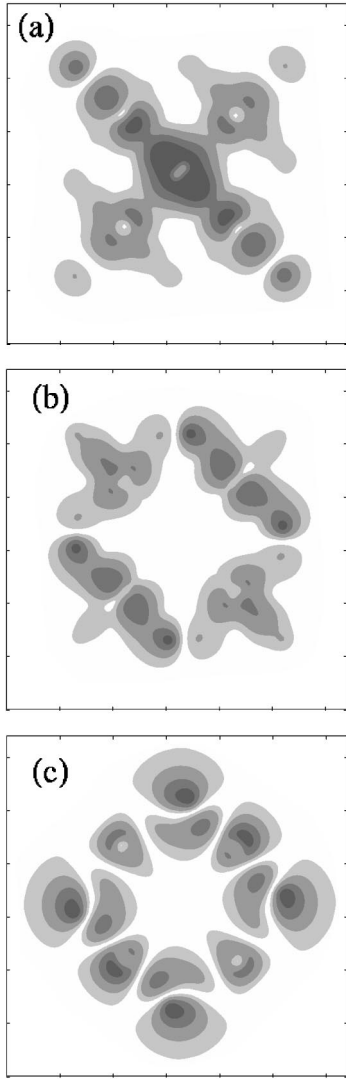


FIG. 5. Contour plot of wave-function squares for the 41-atom Ge nanocrystal. We show the threefold degenerate (and, hence, averaged) second-highest occupied state (a), the threefold degenerate highest occupied state (HOMO) (b), and the nondegenerate lowest unoccupied state (LUMO) (c). A plane through the supercell center normal to a cubic axis is used. Its size corresponds to the edge lengths of the supercell.

present the spectra because the curves are virtually indistinguishable. This result indicates both the validity of Eq. (1) and the fact that our supercell treatments are converged with respect to the cell size. In Fig. 6 we present the resulting spectra $\varepsilon_{nc}(\omega)$ for both Ge and Si. Since $\varepsilon_{host}(\omega) = 1$, formula (1) amounts to a simple scaling of the imaginary parts with the filling factor f . Obviously, quantum size effects have a strong influence on the results. The low-energy sides of the absorption spectra are redshifted with increasing nanocrystal size. Accordingly, with decreasing transition energies the dielectric constants $\text{Re } \varepsilon(\omega = 0)$ become larger.

In contrast to the imaginary parts, the line shape of the real parts of the nanocrystal dielectric functions $\varepsilon_{nc}(\omega)$ in

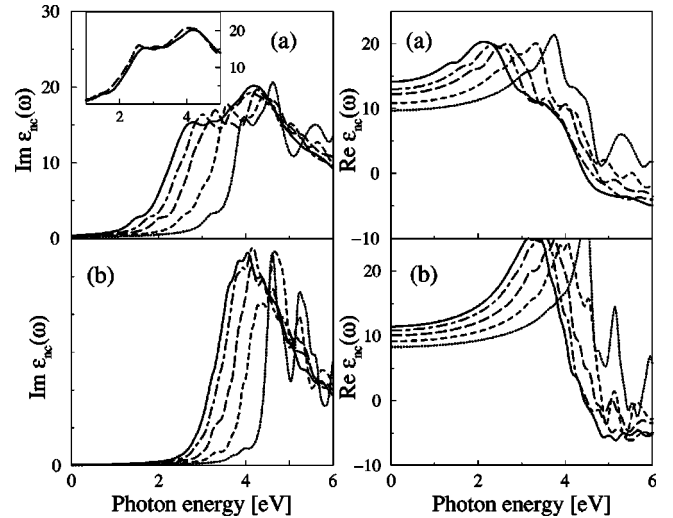


FIG. 6. Nanocrystal dielectric function $\varepsilon_{nc}(\omega)$ of Ge (a) and Si (b) nanocrystallites. $N = 17$, dotted line; $N = 41$, dashed line; $N = 83$, long-dashed line; $N = 147$, dot-dashed line; and $N = 239$, solid line. The insert in (a) shows the absorption spectrum of a 363-atom nanocrystal in comparison with that of the 239-atom cluster.

Fig. 6 are different compared to those of nanocrystals arranged in supercell crystals with vacuum as host material, $\varepsilon(\omega)$ in Fig. 2. The filling factor f does not only give rise to a scaling. We note that the high-frequency dielectric constants for Ge crystallites are, in the given size range, approximated well by a fit formula $\varepsilon_{\infty}^{nc}(R) = 1 + [\varepsilon_{\infty}^{\text{bulk}} - 1] / [1 + (R_0/R)^l]$, which follows from a generalized Penn model.²⁰ Using the fit we find an exponent of approximately $l = 1.1$ for both Ge and Si. The characteristic radii are different with $R_0 = 5.3$ nm (Ge) and $R_0 = 3.5$ nm (Si). For Si, however, the above expression does not provide a very good representation of the calculated values.

For the purpose of comparison with experimental findings, we use the nanocrystal dielectric functions $\varepsilon_{nc}(\omega)$ of Fig. 6 and the Bruggemann effective-medium theory³⁸ (EMT) to calculate optical spectra for Ge nanocrystallites embedded in a host material different from vacuum. We consider an Al_2O_3 matrix with an averaged electronic dielectric constant $\varepsilon_{host}(\omega = 0) = 3.1$.³⁹ In the effective-medium theory of Bruggemann one regards a typical element of the two-phase material, which is embedded in an effective medium, whose properties are to be determined self-consistently. The resulting absorption spectra are presented in Fig. 7 along with experimental results.⁴⁰ Comparing these spectra to the line shape of the absorption spectra of isolated nanocrystallites [cf. Fig. 7(a)], one observes several changes. The peaks are shifted in their energetic position. In particular, the separation increases between the peaks, which develop into the bulk E_1 and E_2 structures. Moreover, the ratio of the peak heights becomes larger for the Ge nanocrystals in sapphire, more strictly speaking the E_1 -like peak is weakened as compared to the E_2 -like peak. The experimental spectra measured for nanocrystallites with an average radius of $R = 1.2$ nm show a similar behavior with respect to the peak separation and the intensity ratio of the peaks. Thus the line shape can qualitatively be correctly described when the

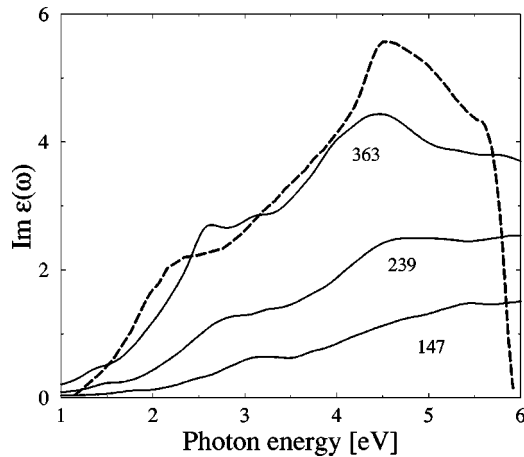


FIG. 7. Spectra of Ge nanocrystals embedded in sapphire (solid lines) calculated by means of Bruggemann EMT from the nanocrystal dielectric function $\epsilon_{nc}(\omega)$. They are compared to an experimental spectrum of Stella *et al.* (Ref. 40) (dashed line). The absolute value of the experimental spectrum is arbitrary. It depends on the filling factor. For generating the theoretical spectra, filling factors of $f = N/1000$ have been used.

effective-medium idea is applied. This means that local fields due to the inhomogeneity of the composite system are important in determining the line shape of optical spectra of composite materials. The comparison with the experimental result shows that the main features of the absorption are already described well, in spite of the simplicity of our structural model and of neglecting important effects such as quasiparticle corrections and excitonic effects. Moreover, we have not attempted to model the size distribution of the nanoparticles in the samples studied experimentally.

Very interesting is the influence of the composition on the peak positions. The shifts of the main absorption peaks, the E_1 - and E_2 -like peaks, are shown with respect to their bulk positions in Fig. 8 for the Ge nanocrystallites embedded in an insulating matrix. While for isolated nanocrystals certain

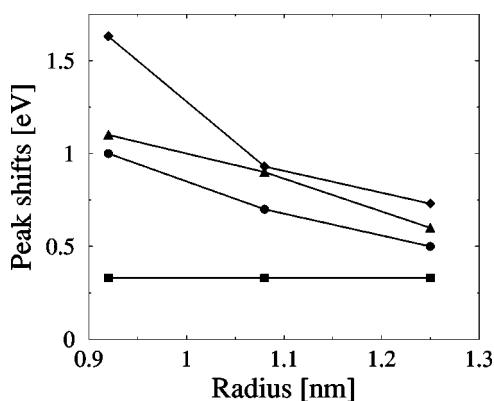


FIG. 8. Shift of the main peaks in the absorption spectra of Ge nanocrystallites with respect to their positions in the corresponding spectrum of Ge bulk. E_1 (dots) and E_2 (squares) of hydrogenated nanocrystals in vacuum, E_1 (triangles) and E_2 (diamonds) of nanocrystals embedded in sapphire. The last values are derived from Bruggemann EMT using filling factors $f = N/1000$.

peak positions, in particular those of E_1 , already show a remarkable dependence on the crystallite size, the effect is seemingly increased after embedding of the nanocrystals in the insulating matrix. Moreover, for isolated nanocrystals the E_2 peak does not exhibit an influence of quantum size effects. For nanocrystallites within the matrix a larger shift towards higher photon energies occurs. However, the physical reasons of this shift are related to local-field effects and not to the spatial quantization of electrons. Consequently, the interpretation of the observed peak shifts²⁴ should be considered with care. A similar conclusion is valid for the comparison of shifts of the E_1 -like peak observed by means of resonance Raman scattering on nanocrystals in SiO_2 (Ref. 28) and transmission spectroscopy on Al_2O_3 samples with Ge nanocrystals. In the two experiments, light is propagating differently and, hence, different local fields are detected. Moreover, careful studies of the confinement influence on the peaks in photoluminescence excitation spectra of Si nanocrystals⁴¹ indicate a complex behavior that can hardly be interpreted in terms of bulk band structures.

IV. CONCLUSIONS

Embedding in a wide-gap material is simulated by a hydrogen saturation of the dangling bonds at the nanocrystal surface. The influence of quantum-confinement effects is much stronger than in the case of a cubic-SiC matrix studied in part I. We have demonstrated the development of the typical optical absorption of nanocrystals towards that known for bulk crystals. It is accompanied by a remarkable increase of the static electronic dielectric constant with the size of the nanocrystallites.

Not only the Kohn-Sham HOMO-LUMO gaps themselves but also the closely related electron-hole pair excitation energies show a strong dependence on the nanocrystal radius. Drastic changes happen for the oscillator strengths of the transitions near the HOMO-LUMO gap. Thereby, Ge and Si nanocrystals behave completely different. While with increasing nanocrystal size the Si nanocrystallites show a tail of weak transitions with decreasing strength, optical transitions with large oscillator strengths occur in Ge nanocrystals near the HOMO-LUMO gap. We traced back these findings to the indirect behavior of Si in the bulk limit and to a representation of the lowest direct E_0 transition of bulk Ge in the Ge case.

We found strong differences between the optical spectra of nanocrystals embedded in vacuum and in an insulating matrix. The local-field effects due to the inhomogeneity in the composite material give rise to considerable changes in the line shape as well as in the peak positions. This has been demonstrated, in particular, for absorption spectra of composite materials in the frequency range of the transitions, which develop into the E_1 and E_2 structures in the bulk limit. The results presented here are in qualitative agreement with experimental observations of optical spectra of Ge dots embedded in a sapphire matrix.

ACKNOWLEDGMENTS

We acknowledge financial support from the Deutsche Forschungsgemeinschaft (Sonderforschungsbereich 196, Project No. A8) and the European Community in the framework of

the Research Training Network NANOPHASE (Contract No. HPRN-CT-2000-00167). Part of the numerical calculations has been done using the facilities of the J. v. Neumann Institute for Computing in Jülich.

- ¹S. Schuppler, S.L. Friedman, M.A. Marcus, D.L. Adler, Y.-H. Xie, F.M. Ross, Y.J. Chabal, T.D. Harris, L.E. Brus, W.L. Brown, E.E. Chaban, P.F. Szajowski, S.B. Christman, and P.H. Citrin, *Phys. Rev. B* **52**, 4910 (1995).
- ²M.V. Wolkin, J. Jorne, P.M. Fauchet, G. Allan, and C. Delerue, *Phys. Rev. Lett.* **82**, 197 (1999).
- ³Y. Maeda, *Phys. Rev. B* **51**, 1658 (1995).
- ⁴S. Takeoka, M. Fujii, S. Hayashi, and K. Yamamoto, *Phys. Rev. B* **58**, 7921 (1998).
- ⁵D.J. Lockwood, *Solid State Commun.* **92**, 101 (1994).
- ⁶L.-W. Wang and A. Zunger, *J. Phys. Chem.* **98**, 2158 (1994).
- ⁷N.A. Hill and K.B. Whaley, *Phys. Rev. Lett.* **75**, 1130 (1995); **76**, 3039 (1996).
- ⁸M. Lannoo, C. Delerue, and G. Allan, *Phys. Rev. Lett.* **74**, 3415 (1995); G. Allan, C. Delerue, M. Lannoo, and E. Martin, *Phys. Rev. B* **52**, 11 982 (1995).
- ⁹Y.M. Niquet, C. Delerue, G. Allan, and M. Lannoo, *Phys. Rev. B* **62**, 5109 (2000).
- ¹⁰B. Delley and E.F. Steigmeier, *Phys. Rev. B* **47**, 1397 (1993); *Appl. Phys. Lett.* **67**, 2370 (1995).
- ¹¹I. Vasiliev, S. Ögüt, and J. R. Chelikowsky, *Phys. Rev. Lett.* **86**, 1813 (2001).
- ¹²S. Ögüt, J.R. Chelikowsky, and S.G. Louie, *Phys. Rev. Lett.* **79**, 1770 (1997).
- ¹³C. Delerue, M. Lannoo, and G. Allan, *Phys. Rev. Lett.* **84**, 2457 (2000).
- ¹⁴R.W. Godby and I.D. White, *Phys. Rev. Lett.* **80**, 3161 (1998).
- ¹⁵A. Franceschetti, L. Wang, and A. Zunger, *Phys. Rev. Lett.* **83**, 1269 (1999).
- ¹⁶S. Ögüt, J.R. Chelikowsky, and S.G. Louie, *Phys. Rev. Lett.* **80**, 3162 (1998); **83**, 1270 (1999).
- ¹⁷M. Rohlfing and S.G. Louie, *Phys. Rev. Lett.* **80**, 3320 (1998).
- ¹⁸R.J. Baierle, M.J. Caldas, E. Molinari, and S. Ossicini, *Solid State Commun.* **102**, 545 (1997).
- ¹⁹M. Palummo, G. Onida, and R. Del Sole, *Phys. Status Solidi A* **175**, 23 (1999).
- ²⁰L.-W. Wang and A. Zunger, *Phys. Rev. Lett.* **73**, 1039 (1994).
- ²¹A. Zunger, *Phys. Status Solidi B* **224**, 727 (2001).
- ²²C. Noguez and S.E. Ulloa, *Phys. Rev. B* **56**, 9719 (1997).
- ²³N. Koshida, H. Koyama, Y. Suda, Y. Yamamoto, M. Araki, T. Saito, K. Sato, N. Sata, and S. Shin, *Appl. Phys. Lett.* **63**, 2774 (1993).
- ²⁴C.E. Bottani, C. Mantini, P. Milani, M. Manfredini, A. Stella, P. Tognini, P. Cheyssac, and R. Kofman, *Appl. Phys. Lett.* **69**, 2409 (1996).
- ²⁵P. Tognini, L.C. Andreani, M. Geddo, A. Stella, P. Cheyssac, R. Kofman, and A. Migliori, *Phys. Rev. B* **53**, 6992 (1996).
- ²⁶P. Tognini, A. Stella, S.D. Silvestri, M. Nisoli, S. Stagira, P. Cheyssac, and R. Kofman, *Appl. Phys. Lett.* **75**, 208 (1999).
- ²⁷P.Y. Yu and M. Cardona, *Fundamentals of Semiconductors* (Springer, Berlin 1995).
- ²⁸K.L. Teo, S.H. Kwok, P.Y. Yu, and S. Guha, *Phys. Rev. B* **62**, 1584 (2000).
- ²⁹H.-Ch. Weissker, J. Furthmüller, and F. Bechstedt, preceding paper, *Phys. Rev. B* **65**, 155327 (2002).
- ³⁰G. Kresse and J. Furthmüller, *Comments Mod. Phys.*, Part C **6**, 1 (1996); *Phys. Rev. B* **54**, 11 169 (1996).
- ³¹B. Adolph, V.I. Gavrilenko, K. Tenelsen, F. Bechstedt, and R. Del Sole, *Phys. Rev. B* **53**, 9797 (1996).
- ³²B. Adolph, J. Furthmüller, and F. Bechstedt, *Phys. Rev. B* **63**, 125108 (2001).
- ³³K.A. Littau, P.J. Szajowski, A.J. Muller, A.R. Kortan, and L.E. Brus, *J. Phys. Chem.* **97**, 1224 (1993).
- ³⁴S. Furukawa and T. Miyasato, *Phys. Rev. B* **38**, 5726 (1988).
- ³⁵S. Schuppler, S.L. Friedman, M.A. Marcus, D.L. Adler, Y.H. Xie, F.M. Ross, T.D. Harris, W.L. Brown, Y.J. Chabal, L.E. Brus, and P.H. Citrin, *Phys. Rev. Lett.* **72**, 2648 (1994).
- ³⁶C.S. Wang and B.M. Klein, *Phys. Rev. B* **24**, 3417 (1981).
- ³⁷S. Albrecht, L. Reining, R. Del Sole, and G. Onida, *Phys. Rev. Lett.* **80**, 4510 (1998); L.X. Benedict, E.L. Shirley, and R.B. Bohn, *ibid.* **80**, 4514 (1998); M. Rohlfing and S.G. Louie, *ibid.* **81**, 2312 (1998).
- ³⁸C.G. Granqvist and O. Hunderi, *Phys. Rev. B* **16**, 3513 (1977).
- ³⁹*Handbook of Chemistry and Physics*, 79th ed., edited by D. R. Lide (CRC Press, Boca Raton, FL, 1998).
- ⁴⁰A. Stella, P. Tognini, P. Cheyssac, R. Kofman, M. Palummo, G. Onida, and R. Del Sole, *Proceedings of the 25th International Conference on Physics of Semiconductors, Osaka, 2000*, edited by N. Miura and T. Ando (Springer, Berlin, 2001), p. 1283.
- ⁴¹M. Ben-Chorin, B. Averboukh, D. Kovalev, G. Polisski, and F. Koch, *Phys. Rev. Lett.* **77**, 763 (1996).